

Deep Gated Networks: A framework to understand training and generalisation in deep learning

Chandrashekhar Lakshminarayanan* and Amit Vikram Singh*,
 Indian Institute of Technology Palakkad
 {chandru@iitpkd.ac.in, amitvikram@gmail.com}

July 17, 2022

Abstract

Understanding the role of (stochastic) gradient descent in training and generalisation of deep neural networks with ReLU activation has been the object of study in the recent past. In this paper, we make use of deep gated networks (DGNs) as a framework to obtain insights about DNNs with ReLU activation. In DGNs, a single neuronal unit has two components namely the pre-activation input (equal to the inner product of the weights of the layer and previous layer outputs), and a gating value which belongs to $[0, 1]$ and the output of the neuronal unit is equal to the multiplication of pre-activation input and the gating value. The standard DNN with ReLU gate, is a special case of the DGNs, wherein the gating value is 1/0 based on whether or not the pre-activation input is positive or negative. We theoretically analyse and experiment with several variants of DGNs, each variant suited to understand a particular aspect of either training/generalisation in DNNs with ReLU activations. Our theory throws light on two questions namely i) why increasing depth till a point helps in training and ii) why increasing depth beyond a point hurts training? We also present experimental evidence to show that gate adaptation is key for generalisation.

1. Introduction

Given a dataset $(x_s, y_s)_{s=1}^n \in \mathbb{R}^{d_{in}} \times \mathbb{R}$, and a deep neural network (DNN), parameterised by $\Theta \in \mathbb{R}^{d_{net}}$, whose prediction on input example $x \in \mathbb{R}^{d_{in}}$ is $\hat{y}_\Theta(x_s) \in \mathbb{R}$, in this paper, we are interested in the stochastic gradient descent (SGD) procedure to minimise the squared loss given by $L_\Theta = \sum_{s=1}^n (\hat{y}_\Theta(x_s) - y_s)^2$. As with some of the recent works [Du et al. \(2018\)](#); [Du and Hu \(2019\)](#) to understand SGD in deep networks we adopt the trajectory based analy-

*Both authors contributed equally.

sis, wherein, one looks at the (error) *trajectory*, i.e., the dynamics of the error defined as $e_t(s) \stackrel{\text{def}}{=} \hat{y}_{\Theta_t}(x_s) - y_s \in \mathbb{R}^n$. The error dynamics is given by:

$$e_{t+1} = e_t - \alpha_t K_t e_t, \quad (1)$$

where $\alpha_t > 0$ is a small enough step-size, $K_t = \Psi_t^\top \Psi_t$ is the $n \times n$ *Gram* matrix, and Ψ is a $d_{net} \times n$ neural tangent feature (NTF) matrix whose entries are given by $\Psi_t(m, s) = \frac{\partial \hat{y}_{\Theta_t}(x_s)}{\partial \theta(m)} \mathbf{1}$ ¹. In particular, we look at the spectral properties of the Gram matrix K_0 for randomised (symmetric Bernoulli) initialisation, and obtain several new insights related to the following:

1. *The Depth Phenomena*: It is well known in practice that increasing depth (of DNNs) till a point improves the training performance. However, increasing the depth beyond a point degrades training.

2. *Gate adaptation*, i.e., the dynamics of the gates in a deep network and its role in generalisation performance.

Conceptual Novelties: In this paper, we bring in two important conceptual novelties. First novelty, is the framework of *deep gated networks* (DGN), previously studied by ([Fiat et al., 2019](#)), wherein, the gating is decoupled from the pre-activation input. Second novelty, is what we call as the *path-view*. We describe these two concepts first, and then explain the gains/insights we obtain from them.

Deep Gated Networks (DGNs): We consider networks with depth d , and a width w (which is the same across layers). A time t , the output $\hat{y}_t(x) \in \mathbb{R}$ of a DGN for an input $x \in \mathbb{R}^{d_{in}}$ can be specified by its gating values and network weights $\Theta_t \in \mathbb{R}^{d_{net}}$ as shown in Table 1.

Θ_t together with collection of the gating values at time t given by $\mathcal{G}_t \stackrel{\text{def}}{=} \{G_{x_s, t}(l, i) \in [0, 1], \forall s \in [n], l \in [d-1], i \in [w]\}$ (where $G(l, i)$ is the gating of i^{th} node in l^{th} layer), we can recover the outputs $\hat{y}_t(x_s)$ for all the inputs $\{x_s\}_{s=1}^n$ in the dataset using the definition in Table 1.

¹We assume that the weights can be enumerated as $\theta(m), m = 1, \dots, d_{net}$.

Input layer	$z_{x,\Theta_t}(0) = x$
Pre-activation	$q_{x,\Theta_t}(l) = \Theta_t(l)^\top z_{x,\Theta_t}(l-1)$
Layer output	$z_{x,\Theta_t}(l) = q_{x,\Theta_t}(l) \odot G_{x,t}(l)$
Final output	$\hat{y}_t(x) = \Theta_t(d)^\top z_{x,\Theta_t}(d-1)$

Table 1. A deep gated network. Here $x \in \mathbb{R}^{d_{in}}$ is the input, and $l = 1, \dots, d-1$ are the intermediate layers. $G_{x_s,t}(l) \in [0, 1]^w$ and $q_{x,\Theta_t}(l) \in \mathbb{R}^w$ are the gating and pre-activation input values respectively at time t .

Path-View: A *path* starts from an input node $i \in [d_{in}]$ ² of the given network, passes through any one of the weights in each layer of the d layers and ends at the output node. Using the paths, we can express the output as the summation of individual path contributions. The path-view has two important gains: i) since it avoids the usual layer after layer approach we are able to obtain explicit expression for information propagation that separates the ‘signal’ from the ‘wire’, (ii) the role of the sub-networks comes out very naturally. Let $x \in \mathbb{R}^{d_{in} \times n}$ denote the data matrix, and let $\Theta_t(l, i, j)$ denote the $(i, j)^{th}$ weight in the l^{th} layer and let $\mathcal{P} = [d_{in}] \times [w]^{d-1}$ be a cross product of index sets. Formally,

- A path p can be defined as $p \stackrel{def}{=} (p(0), p(1), \dots, p(d-1)) \in \mathcal{P}$, where $p(0) \in [d_{in}]$, and $p(l) \in [w], \forall l \in [d-1]$. There are $p = 1, \dots, P = d_{in}w^{d-1}$ paths.
- Strength of a path p is defined as $w_t(p) \stackrel{def}{=} \prod_{l=1}^d \Theta_t(l, p(l-1), p(l))$.
- Activation level of a path p for input x_s is defined as $A_{\mathcal{G}_t}(x_s, p) \stackrel{def}{=} \prod_{l=1}^{d-1} G_{x_s,t}(l, p(l))$.

Conceptual Gain I (Feature Decomposition): Define $\phi_{x_s, \mathcal{G}_t} \in \mathbb{R}^P$, where $\phi_{x_s, \mathcal{G}_t}(p) \stackrel{def}{=} x(p(0), s) A_{\mathcal{G}_t}(x_s, p)$. The output is then given by:

$$\hat{y}_t(x_s) = \phi_{x_s, \mathcal{G}_t}^\top w_t, \quad (2)$$

where $w_t = (w_t(p), p = 1, \dots, P) \in \mathbb{R}^P$. In this paper, $\phi_{x_s, \mathcal{G}_t} \in \mathbb{R}^P$ can be interpreted as *hidden feature* and $w_t \in \mathbb{R}^P$, the strength of the paths can be interpreted as the *weight vector*.

A hard dataset for DNNs: The ability of DNNs to fit data has been demonstrated in the past (Zhang et al., 2016), i.e., they can fit even random labels, and random pixels of standard datasets such as MNIST. However, for standard DNNs with ReLU gates, with no bias parameters, a dataset with $n = 2$ points namely $(x, 1)$ and $(2x, -1)$ for some $x \in \mathbb{R}^{d_{in}}$ cannot be memorised. The reason is that the gating values are the same for both x and $2x$ (for that matter any positive scaling of x), and hence $\phi_{2x, \mathcal{G}_t} = 2\phi_{x, \mathcal{G}_t}$, and

²We use $[d]$ to denote the set $\{1, \dots, d-1\}$

thus it is not possible to fit arbitrary values for $\hat{y}_t(x)$ and $\hat{y}_t(2x)$.

Conceptual Gain II (Similarity Metric): In DGNs similarity of two different inputs $x_s, x_{s'} \in \mathbb{R}^{d_{in}}, s, s' \in [n]$ depends on the overlap of sub-networks that are *active* for both inputs. Let $\Phi_t = [\phi_{x_1, \mathcal{G}_t}, \dots, \phi_{x_n, \mathcal{G}_t}] \in \mathbb{R}^{P \times n}$ be the hidden feature matrix obtained by stacking $\Phi_{x_s, t}, \forall s \in [n]$. Now the Gram matrix M_t of hidden features is given by $M_t = \Phi_t^\top \Phi_t = (x^\top x) \odot \lambda_t$ where $\lambda_t(s, s') \stackrel{def}{=} \sum_{p \sim i} A_{\mathcal{G}_t}(x_s, p) A_{\mathcal{G}_t}(x_{s'}, p)$ ³, stands for the total number of paths that start at any input node i (due to symmetry this number does not vary with $i \in [d_{in}]$) and are *active* for both input examples $s, s' \in [n]$. Each input example has a sub-network that is *active*, and similarity (inner product) of two different inputs depends on the how similar (overlapping between) the corresponding sub-networks that are active for the two inputs.

Conceptual Gain III (Deep Information Propagation): An explicit expression for the Gram matrix as $K_t(s, s') = \sum_{i=1}^{d_{in}} x_s(i) x_{s'}(i) \kappa_t(s, s', i), \forall s, s' \in [n]$. Here, $\kappa_t(s, s', i) \in \mathbb{R}$ is a summation of the inner-products of the *path features* (see Section 2). Thus the input signals $x_s, x_{s'} \in \mathbb{R}^{d_{in}}$ stay as it is in the calculations in an algebraic sense, and are separated out from the wires, i.e., the network whose effect is captured in $\kappa_t(s, s', i)$.

A Decoupling assumption: We assume that the gating \mathcal{G}_0 and weights Θ_0 are statistically independent, and that weights (d_{net} of them) are sampled from $\{-\sigma, +\sigma\}$ with probability $\frac{1}{2}$. Under these assumptions we obtain the following key results and insights:

1. **Depth Phenomena I:** Why does increasing depth till a point helps training?

Because, *increasing depth causes whitening of inputs*. In particular, we show that $\mathbb{E}[K_0] = d\sigma^{2(d-1)} (x^\top x \odot \lambda_0)$, where \odot is the *Hadamard* product. The ratio $\frac{\lambda_0(s, s')}{\lambda_0(s, s)}$ is the fractional overlap of active sub-networks, say at each layer the overlap of active gates is $\gamma \in (0, 1)$, then for a depth d , the fractional overlap decays at exponential rate, i.e., $\frac{\lambda_0(s, s')}{\lambda_0(s, s)} \leq \gamma^d$, leading to whitening.

2. **Depth Phenomena II:** Why does increasing depth beyond a point hurts training?

Because, $Var[K_0(x, x')] \leq O(\max\{\frac{d^2}{w}, \frac{d^3}{w^2}\})$ (for $\sigma^2 = O(\frac{1}{w})$). Thus for large width K_0 converges to its expected value. However, for a fixed width, increasing depth makes the entries of K_0 deviate from $\mathbb{E}[K_0]$, thus degrading the spectrum of K_0 .

³Here $p \sim (\cdot)$ denote the fact that a path p passes through (\cdot) (which is either a node or a weight).

3. Key Take away: To the best of our knowledge, we are the first to present a theory to explain the depth phenomena. While the ReLU gates do not satisfy the decoupling assumption, we hope to relax the decoupling assumption in future and extend the results for decoupled gating to ReLU gates as well.

Conceptual Gain IV (Twin Gradient Flow): The NTF matrix can be decomposed as $\Psi_t(m, s) = \underbrace{\phi_{x_s, \mathcal{G}_t}^\top \frac{\partial w_t}{\partial \theta(m)}}_{\text{strength adaptation}} + \underbrace{\frac{\partial \phi_{x_s, \mathcal{G}_t}^\top}{\partial \theta(m)} w_t}_{\text{gate adaptation}}$, from which it is evident that

the gradient has two components namely i) *strength adaptation*: keeping the sub-networks (at time t) corresponding to each input example fixed, learns the strengths of the paths in those sub-networks, and ii) *gating adaptation*: to learn the sub-networks themselves. Ours is the first work to analytically capture the two gradients.

Conceptual Gain V (Fixing the ReLU artefact): In standard ReLU networks the gates are 0/1 and hence $\frac{\partial \phi_{x_s, \mathcal{G}_t}^\top}{\partial \theta(m)} = 0$. Thus the role of gates has been unaccounted for in the current literature. By parameterising the gates by $\Theta^g \in \mathbb{R}^{d_{\text{net}}}$, and introducing a soft-ReLU gating (with values in $(0, 1)$), we can show that Gram matrix can be decomposed into $K_t = K_t^w + K_t^a$, where K_t^w is the Gram matrix of strength adaptation and K_t^a is the Gram matrix corresponding to activation adaptation. Ours is the first work to point out that the Gram matrix has a gate adaptation component.

- **Conceptual Gain VI (Sensitivity sub-network) :** Our expression for $\mathbb{E}[K_0^a]$ involves what we call *sensitivity* sub-network formed by gates which take intermediate values, i.e., are not close to either 0 or 1. We contend that by controlling such sensitive gates, the DGN is able to learn the features $\phi_{x_s, \mathcal{G}_t}$ over the course of training.

- **Evidence I (Generalisation needs gate adaptation):** We experiment with two datasets namely standard CIFAR-10 (classification) and Binary-MNIST which has classes 4 and 7 with labels $\{-1, +1\}$ (squared loss). We observe that whenever gates adapt, test performance gets better.

- **Evidence II (Lottery is in the gates:)** We obtain 56% test accuracy just by tuning the gates of a parameterised DGN with soft-gates. We also observe that by copying the gates from a learnt network and training the weights from scratch also gives good generalisation performance. This gives a new interpretation for the lottery ticket hypothesis (Frankle and Carbin, 2018), i.e., the real lottery is in the gates.

Lessons Learnt: Rethinking generalisation needs to involve a study on how gates adapt. Taking a cue from (Arora et al., 2019), we look at $\nu_t = y^\top K_t^{-1} y$, and observe that ν_t in the case of adaptive gates/learned gates is always upper

bounded by ν_t when gates are non-adaptive/non-learned gates.

Organisation: The rest of the paper has Section 2, where, we consider DGNs with fixed or frozen gates, and Section 3, where, we look at DGNs with adaptable gates. The idea is obtain insights by progressing stage by stage from easy to difficult variants of DGNs, ordered naturally according to the way in which paths/sub-networks are formed. The proofs of the results are in the supplementary material.

2. Deep Information Propagation in DGN

In this section, we study deep information propagation (DIP) in DGNs when the gates are frozen, i.e., $\mathcal{G}_t = \mathcal{G}_0, \forall t \geq 0$, and our results are applicable to the following:

(i) *Deep Linear Networks (DLN)*: where, all the gating values are 1. Here, we do not have any control over how the paths are formed, since all the paths are *always on*.

(ii) *Fixed random gating (DGN-FRG)*: Note that \mathcal{G}_0 contains $n \times (d-1) \times w$ gating values, corresponding to the n input examples, $(d-1)$ layers and w nodes in each layer. In DGN-FRG, $\mathcal{G}_0 \in \{0, 1\}^{n \times (d-1) \times w}$, where each gating values is chosen to be 0 or 1 with probabilities $1-p$ and p respectively. Here, we have full control over the gating/activation level of the paths. These networks are restricted solely towards understanding questions related to optimisation. Generalisation is irrelevant for DGN-FRG networks because this no natural means to extend the random gate generation for unseen inputs.

(iii) *Gated linear unit (GaLU)*: networks, wherein the gating values are generated by *another separate* network which is DNN with ReLU gates. Unlike DGN-FRG, GaLU networks can generalise.

We first express the Gram matrix K_t in the language of the paths. We then state our assumption in Assumption 2 followed by a main result on deep information propagation in DGNs (Theorem 2.2). We then demonstrate how our main result applies to DGN-FRG and GaLU networks⁴

When the gates are frozen, the weight update affects only the path strengths $w_t(p)$. This is captured as follows:

Sensitivity of path strength with respect to a weight $\theta(m), m \in [d_{\text{net}}]$ in the weights is given by: $\varphi_{t,p}(m) = \prod_{l=1}^d \Theta_t(l, p(l-1), p(l)), \forall p \rightsquigarrow \theta(m)$, and $\varphi_{t,p}(m) = 0, \forall p \not\rightsquigarrow \theta(m)$. The sensitivity of a path p with respect to $\Theta \in \mathbb{R}^{d_{\text{net}}}$ is then given by the vector $\varphi_{t,p} = (\varphi_{t,p}(m), m \in [d_{\text{net}}]) \in \mathbb{R}^{d_{\text{net}}}$.

⁴DLN discussion has been moved to the Supplementary Material in the end.

Singal vs Wire Decomposition: An algebraic Expression for Gram Matrix is given by $K_t(s, s') = \sum_{i=1}^{d_{in}} x(i, s)x(i, s')\kappa_t(s, s', i)$, where, $\kappa_t(s, s', i) \stackrel{\text{def}}{=} \sum_{p_1, p_2 \in P} A_{\mathcal{G}_t}(x_s, p_1)A_{\mathcal{G}_t}(x_{s'}, p_2)\langle \varphi_{t, p_1}, \varphi_{t, p_2} \rangle$, is the amount of overall interaction within the DGN in the i^{th} dimension of inputs $x_s, x_{s'} \in \mathbb{R}^{d_{in}}$. Note that thanks to the path-view the ‘signal’, i.e., $x_s(i)x_{s'}(i)$ gets separated from the ‘wire’ i.e., the connections in the DGN, which is captured in the ‘ κ ’ term. Also, the algebraic expression applies to all DGNs (including the standard DNN with ReLU activations).

Simplifying κ which contains the joint path activity given by $A(x_s, p_1)A(x_{s'}, p_2)$ and the inter-path interaction given by $\langle \varphi_{t, p_1}, \varphi_{t, p_2} \rangle$ is the next step. Towards this end we state and discuss Assumptions 1, 2.

Assumption 1. $\Theta_0 \stackrel{iid}{\sim} \text{Ber}\left(\frac{1}{2}\right)$ over the set $\{-\sigma, +\sigma\}$.

Decoupling of paths from one another, which stands for the fact that the inner product $\langle \varphi_{t, p_1}, \varphi_{t, p_2} \rangle$ of two different paths p_1, p_2 is 0 on expectation. This is captured in Lemma 2.1 below.

Lemma 2.1. Under Assumption 2 we have for paths $p, p_1, p_2 \in \mathcal{P}, p_1 \neq p_2$, at initialisation we have (i) $\mathbb{E}[\langle \varphi_{0, p_1}, \varphi_{0, p_2} \rangle] = 0$, (ii) $\langle \varphi_{0, p}, \varphi_{0, p} \rangle = d\sigma^{2(d-1)}$

Assumption 2. \mathcal{G}_0 is statistically independent of Θ_0 .

Decoupling of gates and paths: In a standard DNN with ReLU activations, the gating and path strengths are statistically dependent because conditioned on the fact that a ReLU is *on*, the incoming weights cannot be simultaneously all *negative*. Assumption 1 makes path strength statistically independent of path activity.

Theorem 2.2 (DIP in DGN). Under Assumption 2, and $\frac{4d}{w^2} < 1$ it follows that

$$\mathbb{E}[K_0] = d\sigma^{2(d-1)}(x^\top x \odot \lambda_0)$$

$$\text{Var}[K_0] \leq O\left(d_{in}^2\sigma^{4(d-1)} \max\{d^2w^{2(d-2)+1}, d^3w^{2(d-2)}\}\right)$$

Choice of σ : Note that in the case of gates taking values in $\{0, 1\}$, $\lambda_0(s, s'), s, s' \in [n]$, is a measure of overlap of sub-networks that start at any given input node, end at the output node, and are active for both input examples s, s' . Loosely speaking, say in each layer $\gamma \in (0, 1)$ fraction of the gates are *on*, then $\lambda_0(s, s)$ is about $(\gamma w)^{d-1}$. Thus, to ensure that the signal does not blow up with a DGN, we need to $(\sigma^2\gamma w)^{d-1} = 1$, which means $\sigma = O\left(\sqrt{\frac{1}{\gamma w}}\right)$. In our experiments, we set $\sigma = \sqrt{\frac{2}{w}}$.

In the expression for $\mathbb{E}[K_0]$ note that the input Gram matrix $x^\top x \in \mathbb{R}^{n \times n}$ is separate from $\lambda_0 \in \mathbb{R}^{n \times n}$ which is a

Gram matrix of the active sub-networks. Thanks to the path-view, we do not lose track of the input information which is otherwise bound to happen if we were to choose a layer by layer view of DIP in DGNs.

Fixed Random Gating (DGN-FRG) involves sampling the gates \mathcal{G}_0 from $\text{Ber}\left(\frac{1}{2}\right)$, and hence there is a random sub-network which is active for each input. Under FRG, we can obtain closed form expression for the ‘ $\lambda(\cdot, \cdot, \cdot)$ ’ term as below:

Lemma 2.3. Under Assumption 1, 2 and gates sampled iid $\text{Ber}(p)$, we have, $\forall s, s' \in [n]$

- (i) $\mathbb{E}_p[\lambda_0(s, s)] = \bar{\lambda}_{self} = d(pw)^{d-1}$
- (ii) $\mathbb{E}_p[\lambda_0(s, s')] = \bar{\lambda}_{cross} = d(p^2w)^{d-1}$

DIP in DGN-FRG: For $\sigma = \sqrt{\frac{1}{pw}}$, we have:

$$\frac{\mathbb{E}[K_0]}{d} = \begin{bmatrix} \cdot & \cdot & \cdot & \cdot & \cdot \\ \cdot & \langle x_s, x_s \rangle & \cdot & \langle x_s, x_{s'} \rangle p^{d-1} & \cdot \\ \cdot & \langle x_{s'}, x_s \rangle p^{d-1} & \cdot & \langle x_{s'}, x_{s'} \rangle & \cdot \\ \cdot & \cdot & \cdot & \cdot & \cdot \end{bmatrix}$$

Experiment 1: Consider the dataset $(x_s, y_s)_{s=1}^n \in \mathbb{R} \times \mathbb{R}$, where $x_s = 1, \forall s \in [n]$, and $y_s \sim \text{unif}([-1, 1])$, $n = 200$. The input Gram matrix $x^\top x$ is a $n \times n$ matrix with all entries equal to 1 and its rank is equal to 1. This is the worst possible case for optimisation, since all the inputs are identical.

Why increasing depth till a point helps? In the case of Experiment 1, we have:

$$\frac{\mathbb{E}[K_0]}{d} = \begin{bmatrix} 1 & p^{d-1} & \dots & p^{d-1} & \dots \\ \dots & 1 & \dots & p^{d-1} & \dots \\ \dots & p^{d-1} & \dots & 1 & \dots \\ \dots & p^{d-1} & \dots & p^{d-1} & 1 \end{bmatrix} \quad (3)$$

i.e., all the diagonal entries are 1 and non-diagonal entries are p^{d-1} . Now, let $\rho_i \geq 0, i \in [n]$ be the eigenvalues of $\frac{\mathbb{E}[K_0]}{d}$, and let ρ_{\max} and ρ_{\min} be the largest and smallest eigenvalues. From the structure of (3), one can easily show that $\rho_{\max} = 1 + (n-1)p^{d-1}$ and corresponds to the eigenvector with all entries as 1, and $\rho_{\min} = (1-p^{d-1})$ repeats $(n-1)$ times, which corresponds to eigenvectors given by $[0, 0, \dots, \underbrace{1, -1, \dots, 0, 0, \dots, 0}_i, 0]^\top \in \mathbb{R}^n$ for $i = 1, \dots, n-1$.

Why increasing depth beyond a point hurts? In Theorem 2.2, note that for a fixed width w , as the depth increases the variance of the entries $K_0(s, s')$ deviates from its expected value $\mathbb{E}[K_0(s, s')]$. Thus the structure of the Gram matrix degrades from (3), leading to smaller eigenvalues.

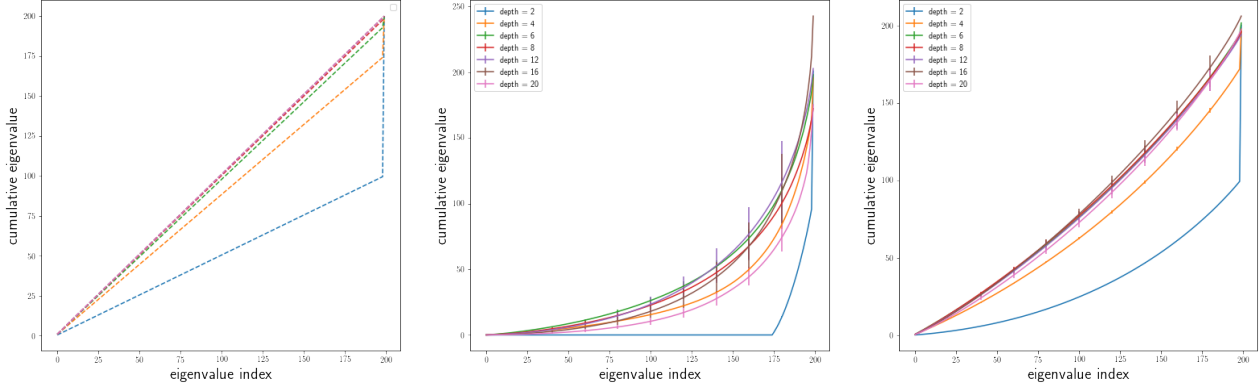


Figure 1. Shows the plots for DGN-FRG with $p = \frac{1}{2}$ and $\sigma = \sqrt{\frac{2}{w}}$. The first plot in the left shows the ideal cumulative eigenvalue (e.c.d.f) for various depths $d = 2, 4, 6, 8, 12, 16, 20$. Note that the ideal plot converges to identity matrix as d increases. The second and third plot (from the left), plots respectively show the cumulative eigenvalues (e.c.d.f) for $w = 500$ and $w = 25$ respectively. Note that the e.c.d.f of higher width $w = 500$ is better conditioned than the e.c.d.f of $w = 25$.

Numerical Evidence (Gram Matrix): We first fix arbitrary diagonal and non-diagonal entries, and look at their value averaged over 20 run (see Figure 2). The actual values shown in bold indeed follow the ideal values shown in the dotted lines and the values are as per (3)).

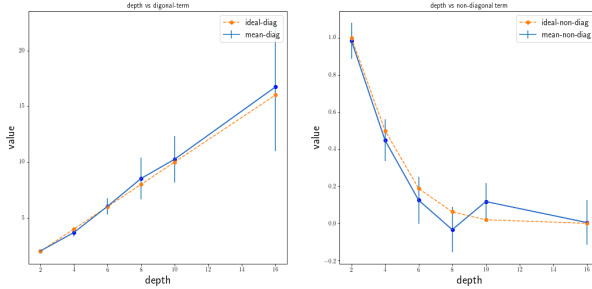


Figure 2. For $w = 500$, and $p = 0.5$, (an arbitrary) diagonal (left plot) and non-diagonal (right plot) of the Gram matrix K_0 for dataset in Experiment 1 is shown. The plots are averaged over 20 runs.

Numerical Evidence (Spectrum): Next, we look at the cumulative eigenvalue (e.c.d.f) obtained by first sorting the eigenvalues in ascending order then looking at their cumulative sum. The ideal behaviour (middle plot of Figure 1) as predicted from theory is that for indices $k \in [n - 1]$, the e.c.d.f should increase at a linear rate, i.e., the cumulative sum of the first k indices is equal to $k(1 - p^{d-1})$, and the difference between the last two indices is $1 + (n - 1)p^{d-1}$. In Figure 1, we plot the e.c.d.f for various depths $d = 2, 4, 6, 8, 12, 16, 20$ and two different width namely $w = 25, 500$. It can be seen that as w increases, the difference between the ideal and actual e.c.d.f curves is less ($w = 500$ when compared to $w = 25$).

Numerical Evidence (Role of Depth): In order to compare

how the rate of convergence varies with the depth in DGN-FRG network, we set the step-size $\alpha = \frac{0.1}{\rho_{\max}}$, $w = 100$, and fit data described in **Experiment 1**. We use the vanilla SGD-optimiser. Note that it follows from (1) that the convergence rate is determined by a linear recursion, and choosing $\alpha = \frac{0.1}{\rho_{\max}}$ can be seen to be equivalent to having a constant step-size of $\alpha = 0.1$ but dividing the Gram matrix by its maximum eigenvalue instead. Thus, after this rescaling, the maximum eigenvalue is 1 uniformly across all the instances, and the convergence should be limited by the smaller eigenvalues. We also look at the convergence rate of the ratio $\frac{\|e_t\|_2^2}{\|e_0\|_2^2}$, and we observe that the convergence rate gets better with depth as predicted by theory (Figure 3).

GaLU Networks: Here the gating values are obtained from a DNN with ReLU activation, parameterised by $\Theta^g \in \mathbb{R}^{d_{\text{net}}}$ (these weights are frozen). Due to the symmetric nature of the weights, we can expect roughly half the number of gates to be *on*, and it follows that $\bar{\lambda}_{\text{self}}(s) \approx d(\gamma\sigma^2)^{d-1}$ with $\gamma \approx \frac{1}{2}$. By defining $\bar{\lambda}_{\text{self}}(s) \stackrel{\text{def}}{=} \mathbb{E}_{\Theta_0^g} [\lambda_0(s, s)]$, and $\bar{\lambda}_{\text{cross}}(s, s') \stackrel{\text{def}}{=} \mathbb{E}_{\Theta_0^g} [\lambda_0(s, s')]$, and $\eta = \max_{s, s' \in [n]} \frac{\bar{\lambda}_{\text{cross}}(s, s')}{\bar{\lambda}_{\text{self}}(s)}$, we can see that while the non-diagonal entries of the $\mathbb{E}[K_0]$ decay at a different rates, the rate of decay is nonetheless upper bounded by η^{d-1} . Note that in DGN-FRG decay of non-diagonal terms is at a uniform rate given by p^{d-1} .

Experiment 2: To characterise the optimisation performance of GaLU and ReLU networks, we consider dataset $(x_s, y_s)_{s=1}^n \in \mathbb{R}^2 \times \mathbb{R}$, where, $x_s \stackrel{iid}{\sim} \text{unif}([-1, 1]^2)$ and $y_s \stackrel{iid}{\sim} \text{unif}([-1, 1])$, $n = 100$. The results are shown in Figure 4. The rationale behind choosing this data set is that we want the inputs to be highly correlated by choice.

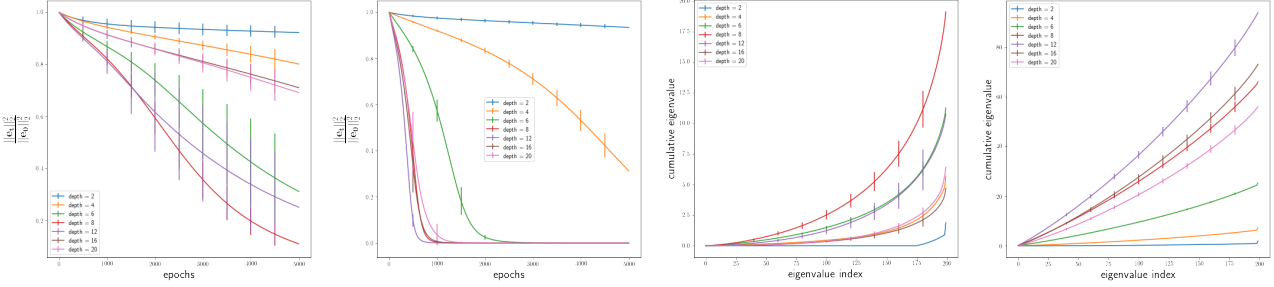


Figure 3. Shows the plots for DGN-FRG. The left two plots show the convergence rates for $w = 25$ and $w = 500$. The right two values are showing the e.c.d.f obtained by first dividing the Gram matrix by their maximum eigenvalue. The plots are averaged over 5 runs.

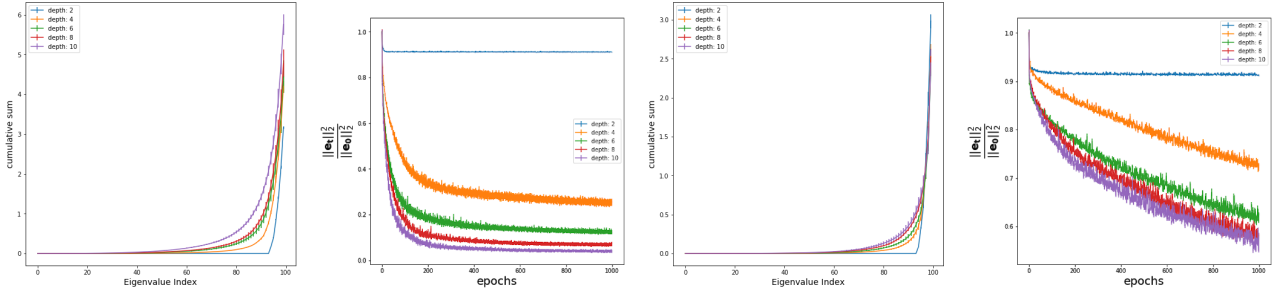


Figure 4. The left two plots shows the e.c.d.f and convergence rates for various depth in GaLU networks $w = 100$. The third and fourth plot from the left show the e.c.d.f and convergence rates for various depth in ReLU networks $w = 100$. The plots are averaged over 5 runs.

GaLU Networks (Depth helps in training): The trend is similar to DGN-FRG case, in that, both e.c.d.f as well as convergence get better with increasing depth. Here too we set the stepsize $\alpha = \frac{0.1}{\rho_{\max}}$ (and vanilla SGD). We also observe that in **Experiment 2** *GaLU networks optimise better than standard ReLU networks*, and it is also true that the e.c.d.f for the case of GaLU is better than that of ReLU. This can be attributed to the fact that, in ReLU network the dot product of two different active paths is not zero and hence the Gram matrix entries fall back to the vanilla algebraic expression for K_t .

3. Generalisation

ReLU networks generalise better than GaLU: We trained both ReLU and GaLU networks on standard MNIST dataset to 100% accuracy. We observed that the GaLU network trains a bit faster than the ReLU network (see Figure 5). However, in test data we obtain accuracy of around 96.5% and 98.5% for GaLU and ReLU networks respectively. A key difference between GaLU and ReLU networks is that in ReLU networks the gates are adapting, i.e., \mathcal{G}_t keeps changing with time. This leads us to the following natural question:

Is gate adaptation key for generalisation performance?

Hidden features are in the sub-networks and are

learned: We consider ‘‘Binary’’-MNIST data set with two classes namely digits 4 and 7, labels taking values in $\{-1, +1\}$ and squared loss. We trained a standard DNN with ReLU gates ($w = 100$, $d = 5$). Recall from Section 1 that $M_t = \Phi_t^\top \Phi_t$ the Gram matrix of the features, and let $\widehat{M}_t = \frac{1}{\text{trace}(M_t)} M_t$ be its normalised counterpart. For a subset size, $n' = 200$ (100 examples per class) we plot $\nu_t = y^\top (\widehat{M}_t)^{-1} y$, (where $y \in \{-1, 1\}^{200}$ is the labeling function), and observe that ν_t reduces as training proceeds (see middle plot in Figure 6). Note that $\nu_t = \sum_{i=1}^{n'} (u_{i,t}^\top y)^2 (\hat{\rho}_{i,t})^{-1}$, where $u_{i,t} \in \mathbb{R}^{n'}$ are the orthonormal eigenvectors of \widehat{M}_t and $\hat{\rho}_{i,t}, i \in [n']$ are the corresponding eigenvalues. Since $\sum_{i=1}^{n'} \hat{\rho}_{i,t} = 1$, the only way ν_t reduces is when more and more energy gets concentrated on $\hat{\rho}_{i,t}$ s for which $(u_{i,t}^\top y)^2$ s are also high. However, in $M_t = (x^\top x) \odot \lambda_t$, only λ_t changes with time. Thus, $\lambda_t(s, s')$ which is a measure of overlap of sub-networks active for input examples $s, s' \in [n]$, changes in a manner to reduce ν_t . We can thus infer that the *right* active sub-networks are learned over the course of training.

DGNs with adaptable gates: To investigate the role of gate adaptation, we study parameterised DGNs of the general form given in Table 2. The specific variants we study in the experiments are in Table 3.

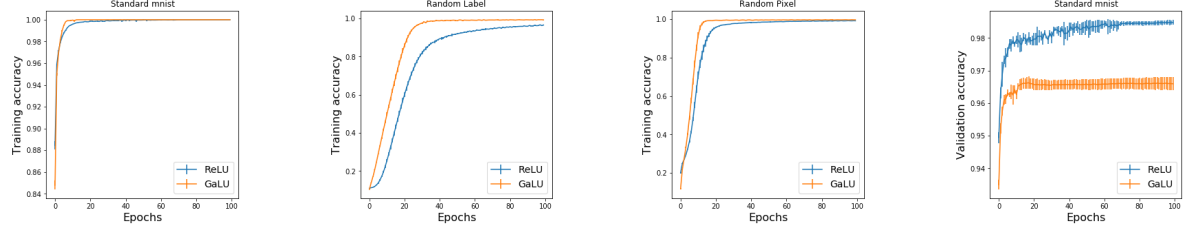


Figure 5. Shows optimisation in ReLU and GaLU networks for standard MNIST, MNIST with random label and pixels (first three from the left). The right most plot shows generalisation of ReLU and GaLU networks in standard MNIST. Architecture we use is $d = 7$, with layer widths from the first to last given by 512, 512, 256, 256, 128, 64, 10 followed by a soft-max layer. In the case of GaLU there are two such network, wherein, one network is used to generate the gating values (whose weights are frozen) and the other network has the weights that are trained.

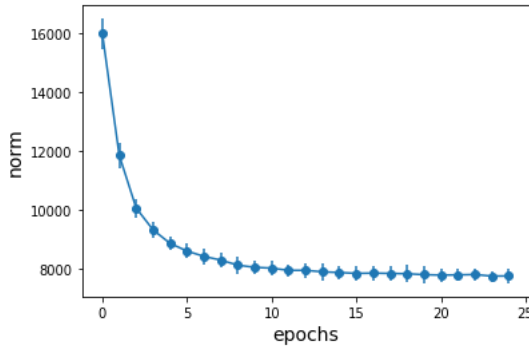


Figure 6. Shows $\nu_t = y^T (\widehat{M}_t)^{-1} y$, where $M_t = \Phi_t^\top \Phi_t$.

Gating Network	Weight Network
$z_{x,\Theta_t^g}(0) = x$	$z_{x,\Theta_t^w}(0) = x$
$q_{x,\Theta_t^g}(l) = \Theta_t^g(l)^\top z_{x,\Theta_t^g}(l-1)$	$q_{x,\Theta_t^w}(l) = \Theta_t^w(l)^\top z_{x,\Theta_t^w}(l-1)$
$z_{x,\Theta_t^g}(l) = q_{x,\Theta_t^g}(l) \odot G_{x,\Theta_t^g}(l)$	$z_{x,\Theta_t^w}(l) = q_{x,\Theta_t^w}(l) \odot G_{x,\Theta_t^w}(l)$
$\hat{y}_t(x) = \Theta_t^w(d)^\top z_{x,\Theta_t^w}(d-1)$	
$\beta > 0 : G_{x,\Theta_t^g}(l) = \chi_\varepsilon(-\beta q_{x,\Theta_t^g}(l)),$	
$\beta = \infty : G_{x,\Theta_t^g}(l) = \mathbb{1}_{\{q_{x,\Theta_t^g}(l) > 0\}}$	

Table 2. A DGN with parameterised gates. Here, for $\varepsilon \geq 0$, $\chi_\varepsilon(v) = \frac{1+\varepsilon}{1+\exp(v)}$, $\forall v \in \mathbb{R}$

We now explain the idea behind the various gates (and some more) in Table 3 as follows:

1. The most general gate is called the *soft-GaLU* gate denoted by $\mathcal{N}(\Theta_t^g, \beta; \Theta_t^w)$. Here, gating and hence the path activation levels are decided by $\Theta_t^g \in \mathbb{R}^{d_{net}}$, and path strengths are decided by $\Theta_t^w \in \mathbb{R}^{d_{net}}$. This network has $2 \times d_{net}$ parameters.
2. The standard DNN with ReLU gating is denoted by $\mathcal{N}(\Theta_t, \infty; \Theta_t)$, where ∞ signifies that the outputs are 0/1 (see Table 2), and the fact that $\Theta_t \in \mathbb{R}^{d_{net}}$ appears twice signifies the fact that both gating (and hence path activation levels) and path strengths are decided by the same parameter namely $\Theta_t \in \mathbb{R}^{d_{net}}$.

Terminology	Notation	Remarks
ReLU	$\mathcal{N}(\Theta_t, \infty; \Theta_t)$	$\Theta_t \in \mathbb{R}^{d_{net}}$
GaLU (Frozen)	$\mathcal{N}(\Theta_t^g, \infty; \Theta_t^w)$	$\Theta_t^w \in \mathbb{R}^{d_{net}}$, $\Theta_t^g \in \mathbb{R}^{d_{net}}$
Soft-ReLU	$\mathcal{N}(\Theta_t, \beta; \Theta_t)$	$G \in (0, 1)$ (not decoupled)
Soft-GaLU	$\mathcal{N}(\Theta_t^g, \beta; \Theta_t^w)$	$G \in (0, 1)$ (decoupled)

Table 3. Shows the variants of DGNs in the experiments. Here, \dagger stands for frozen weights that are initialised by not trained.

3. $\mathcal{N}(\Theta_t, \beta; \Theta_t)$ is a DNN with what we call the *soft-ReLU* gates, where the gating values are in $(0, 1 + \varepsilon)$ instead of 0/1. Here too like standard ReLU networks, both gating and path strengths are decided by $\Theta_t \in \mathbb{R}^{d_{net}}$.

4. $\mathcal{N}(\Theta_t^g, \infty; \Theta_t^w)$ is what we call a GaLU-frozen DGN, where the gating parameters $\Theta_t^g \in \mathbb{R}^{d_{net}}$ are initialised but not trained.

5. $\mathcal{N}(\Theta_t^g, \beta; \Theta_t^w)$ is a network where only the gating parameters $\Theta_t^g \in \mathbb{R}^{d_{net}}$ are trainable and the parameters which dictate the path strengths namely Θ_t^w are initialised by not trained.

Gradient of gate adaptation

• **Fixing ReLU artefact:** We refer to the function $\chi_\varepsilon(v)$ in Table 2 as the *soft* gating function. Note that, the NTF has two components given by $\Psi_t(m, s) = \phi_{x_s, G_t}^\top \frac{\partial w_t}{\partial \theta(m)} + \frac{\partial \phi_{x_s, G_t}^\top}{\partial \theta(m)} w_t$. Since in ReLU networks the gates are either 0/1, the activation level are also 0/1 and hence their derivative is 0. In contrast, the soft-gating is differentiable, and hence the $\frac{\partial \phi_{x_s, G_t}^\top}{\partial \theta(m)} w_t \neq 0$ and is accounted in the analysis.

• **For soft-GaLU:** Since there are two set of parameters (total $2d_{net}$) $\Psi^\top = [\Psi_t^w, \Psi_t^a]^\top$ is a $n \times 2d_{net}$, we have $K_t = K_t^w + K_t^a$, where $K_t^w = \Psi_t^w \top \Psi_t^w$, and $K_t^a = \Psi_t^a \top \Psi_t^a$.

• **For soft-ReLU:** $K_t = K_t^w + K_t^a + \Psi_t^w \top \Psi_t^a + \Psi_t^a \top \Psi_t^w$.

Definition 3.1. Using any $i \in [d_{in}]$, define $\delta(s, s') \stackrel{\text{def}}{=}$

$$\sum_{p \sim i} \sum_{m=1}^{d_{net}} \frac{\partial A_{\Theta_0^g}(x_s, p)}{\partial \theta^g(m)} \frac{\partial A_{\Theta_0^g}(x_{s'}, p)}{\partial \theta^g(m)}.$$

Lemma 3.1. Under Assumptions 1, 2, in soft-GaLU networks we have: (i) $\mathbb{E}[K_0] = \mathbb{E}[K_0^w] + \mathbb{E}[K_0^a]$, (ii) $\mathbb{E}[K_0^w] = \sigma^{2(d-1)}(x^\top x) \odot \lambda$, (iii) $\mathbb{E}[K_0^a] = \sigma^{2d}(x^\top x) \odot \delta$

Adaptable gates generalise better: In all experiments below, we use step-size $\alpha = 1e^{-4}$, $w = 100$, $d = 6$ and we use RMSprop to train.

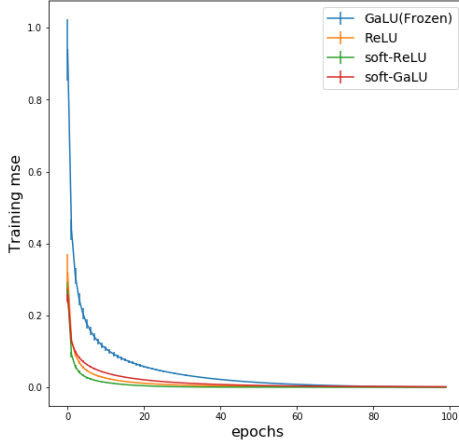


Figure 7. Shows the training performance of the 4 different networks in **Experiment 3** with $w = 100$, $d = 6$.

• **Experiment 3:** On 'Binary'-MNIST, We train four different networks ($w = 100$, $d = 6$), namely, $\mathcal{N}(\Theta_t^g, \beta = 4; \Theta_t^w)$ (soft-GaLU), $\mathcal{N}(\Theta_t, \beta = 4; \Theta_t)$ (soft-ReLU), $\mathcal{N}(\Theta_t, \infty; \Theta_t^w)$ (ReLU), and $\mathcal{N}(\Theta_t^g, \infty; \Theta_t^w)$ (GaLU with frozen gates). We observe that the networks with adaptable gates generalise better as shown in Figures 7 and 8.

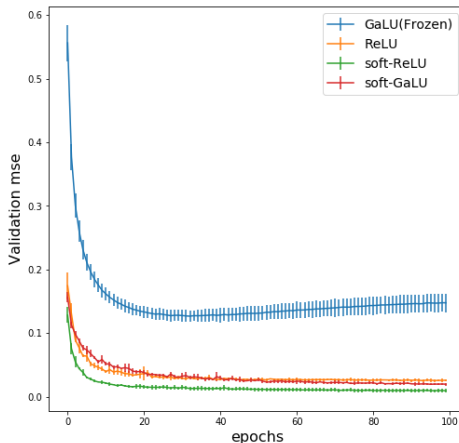


Figure 8. Shows the generalisation performance of the 4 different networks in **Experiment 3** with $w = 100$, $d = 6$.

• **Experiment 4:** We train a frozen ReLU network $\mathcal{N}(\Theta_t^g, \infty; \Theta_t^w)$, where $\Theta_0^g = \Theta_0^w$ (weights chosen according to Assumption 2), and a standard ReLU network $\mathcal{N}(\Theta_t, \infty; \Theta_t)$ in which the gates adapt. We observe that generalisation is better when the gates adapt (see Figure 9).

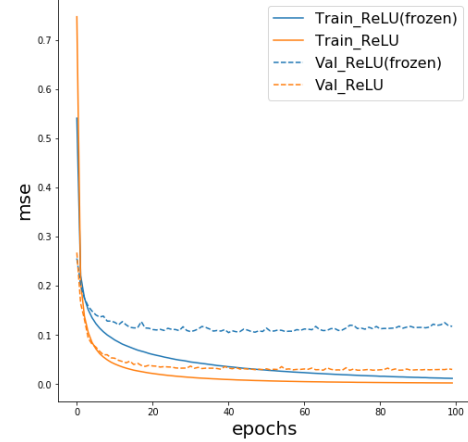


Figure 9. **Experiment 4** with $w = 100$, $d = 6$. Generalisation performance (dotted lines) adaptable gates is better than frozen gates. The training performance is shown in bold lines. The plots are averaged over 5 runs.

• **Experiment 5 (Lottery Ticket):** We train $\mathcal{N}(\Theta_t, \infty; \Theta_t)$ (a standard DNN with ReLU gates) till time $T = 100$ epochs. We then use the weights to initialise $\Theta_0^g = \Theta_T$ for the network $\mathcal{N}(\Theta_t^g, \infty; \Theta_t^w)$ and train Θ_t^w (initialised independently) and we call this GaLU with learned gates. We also consider the case of GaLU network with non-learned gates, where we train $\mathcal{N}(\Theta_t^g, \infty; \Theta_t^w)$ where Θ_0^g and Θ_0^w is initialised according to Assumptions 1, 2. We observe that the learned gates generalise better than the unlearned case (see Figure 10). This shows that the real lottery is in the gates.

• **Experiment 6 (Lottery Ticket):** We consider $\mathcal{N}(\Theta_t^g, \infty; \Theta_t^w)$, where the weights corresponding to the strengths Θ^w are frozen, but the weights Θ^g that parameterise the gates are trained. We observed a 56% test performance in CIFAR-10 just by tuning the gates. For this experiment, we used a *convolutional* neural network, of the following architecture: input layer is $(32, 32, 3)$, followed by $conv(3, 3) : 64, 64, 128, 128$, followed by $Flatten()$, $256, 256, 10$.

• **Measure for generalisation:** In order to look for a possible explanation for the better generalisation, we plot $\nu_t = y^\top (H_t)^{-1} y$ (for various choices of H_t , see Figures 11 to 14), for the Binary-MNIST in Experiment 3. We observe that ν_t is smaller for the learned/adaptable gates when compared respectively to the case of non-learned/frozen gates. The behaviour of ν_t points to the fact that when gates adapt,

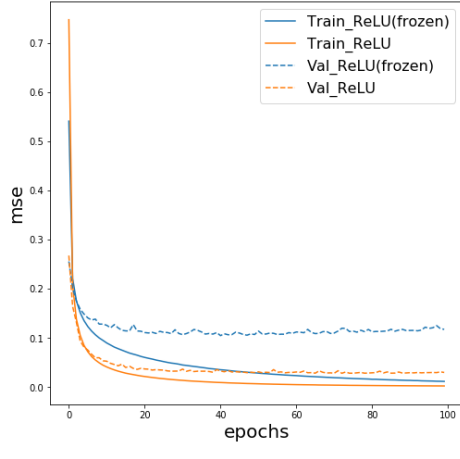


Figure 10. **Experiment 5** with $w = 100$, $d = 6$. Generalisation performance (dotted lines) of learned gates is better than ‘non’-learned gates. The training performance is shown in bold lines. The plots are averaged over 5 runs.

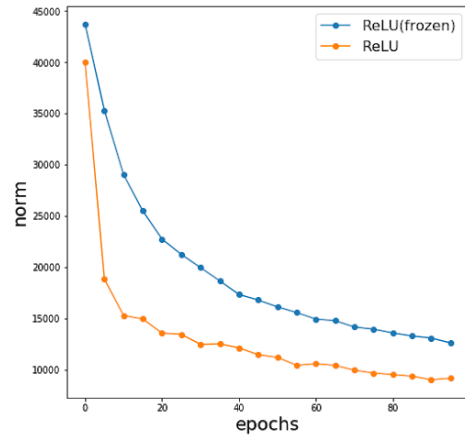


Figure 12. Shows $\nu_t = y^\top (H_t)^{-1} y$ for $H_t = \widehat{K}_t$.

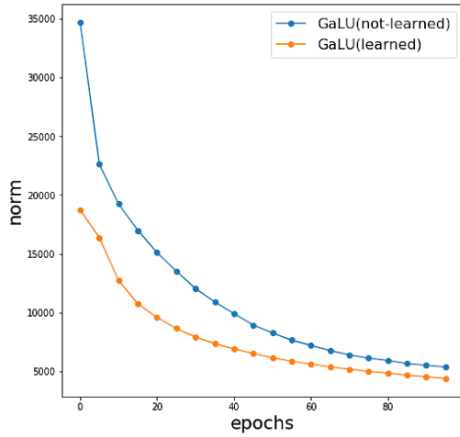


Figure 11. Shows $\nu_t = y^\top (H_t)^{-1} y$ for $H_t = K_t$.

the underlying Gram matrices align their eigen-space in accordance with the labeling function.

• **Experiment 7:** We train convolution networks with soft-ReLU gates (i.e., $\chi_\varepsilon(v)$) for various values of β and ε on CIFAR-10 dataset. For moderately high values of β we obtain generalisation performance of 72% which is comparable to what we obtain for DNNs (identical architecture, and hyper-parameters) with standard ReLU gates (see in supplementary material).

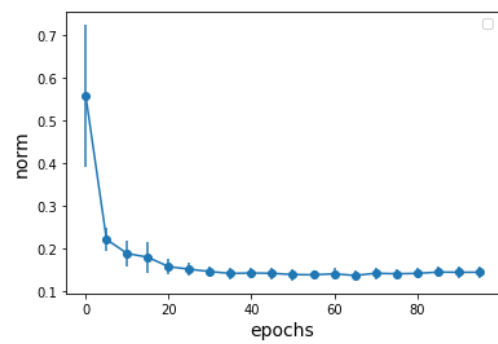


Figure 13. Shows $\nu_t = y^\top (H_t)^{-1} y$ for $H_t = K_t^a$. Here, K_t^a is the Gram matrix of activations in the soft-GaLU network.

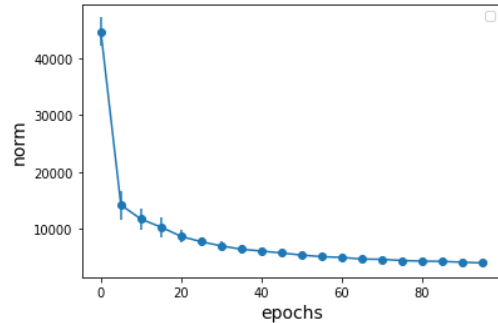


Figure 14. Shows $\nu_t = y^\top (H_t)^{-1} y$ for $H_t = \widehat{K}_t^a$. Here, K_t^a is the Gram matrix of activations in the soft-GaLU network.

Network	Training Accuracy	Test Accuracy
Deep Linear Network	0.5042	0.3939
Relu	0.99	0.71
$\beta = 1, \varepsilon = 0.1$	0.99	0.59
$\beta = 2, \varepsilon = 0.1$	0.99	0.64
$\beta = 4, \varepsilon = 0.1$	0.99	0.68
$\beta = 8, \varepsilon = 0.1$	0.99	0.71
$\beta = 12, \varepsilon = 0.1$	0.99	0.71
$\beta = 16, \varepsilon = 0.1$	0.99	0.72
$\beta = 20, \varepsilon = 0.1$	0.99	0.72
$\beta = 24, \varepsilon = 0.1$	0.99	0.72
$\beta = 1, \varepsilon = 0.4$	0.99	0.56
$\beta = 2, \varepsilon = 0.4$	0.99	0.63
$\beta = 4, \varepsilon = 0.4$	0.99	0.68
$\beta = 8, \varepsilon = 0.4$	0.99	0.71
$\beta = 12, \varepsilon = 0.4$	0.99	0.71
$\beta = 16, \varepsilon = 0.4$	0.99	0.71
$\beta = 20, \varepsilon = 0.4$	0.99	0.71
$\beta = 24, \varepsilon = 0.4$	0.99	0.71

Table 4. Shows performance of various networks for CIFAR 10 dataset. The results are averaged over 5 runs. The reported results are mean of the best performance obtained in each run.

3.1. Preliminary analysis of gate adaptation:

Recall that $\mathcal{G}_t \stackrel{\text{def}}{=} \{G_{x_s, t}(l, i) \in [0, 1], \forall s \in [n], l \in [d-1], i \in [w]\}$. We now define the following:

- **Active Gates:** For an input $x_s \in \mathbb{R}^{d_{in}}$, and a threshold value $\tau_A \in (0, 1 + \varepsilon)$, define $\mathcal{G}_t^A(x_s, \tau_A) \stackrel{\text{def}}{=} \{G_{x_s, t}(l, i) : G_{x_s, t}(l, i) > \tau_A, l \in [d-1], i \in [w]\}$. These are the gates that are *on* (i.e., more than threshold τ_A) for input $x_s \in \mathbb{R}^{d_{in}}$.
- **Sensitive Gates:** For an input $x_s \in \mathbb{R}^{d_{in}}$, and a threshold value $\tau_S > 0$, define $\mathcal{G}_t^S(x_s, \tau_S) \stackrel{\text{def}}{=} \bigcup_{m=1}^{d_{net}} \left\{ G_{x_s, t}(l, i) : \left| \frac{\partial G_{x_s, t}(l, i)}{\partial \theta^g(m)} \right| > \tau_S, l \in [d-1], i \in [w] \right\}$. These are set of gates that are sensitive to changes in anyone of the $\theta^g(m), m \in [d_{net}]$ tunable parameters that control the gates.
- **Relation between sensitive and active gates:** From the nature of the soft-gating function $\chi_\varepsilon(v)$ it follows that for any given $\tau_A \in (0, 1 + \varepsilon)$, it follows that $\mathcal{G}_t^A(x_s, \tau_A) \cap \mathcal{G}_t^S(x_s, \tau_S) = \emptyset, \forall \tau_S > \frac{d\chi_\varepsilon(v)}{dv} \Big|_{v=\chi_\varepsilon^{-1}(v)}$. Also, note that as $\tau_A \rightarrow (1 + \varepsilon)$, $\tau_S \rightarrow 0$.
- **Sensitivity of Activations:** For a path p , and a gating parameter $\theta^g(m), m \in [d_{net}]$ we have $\frac{\partial A_{\Theta_t^g(x_s, p)}}{\partial \theta^g(m)}$ to be equal to

$$\sum_{l=1}^{d-1} \left(\frac{\partial G_{x_s, \Theta_t^g}(l, p(l))}{\partial \theta^g(m)} \right) \left(\prod_{l' \neq l} G_{x_s, \Theta_t^g}(l', p(l')) \right) \quad (4)$$

In what follows we assume that $\tau_S > \frac{d\chi_\varepsilon(v)}{dv} \Big|_{v=\chi_\varepsilon^{-1}(v)}$.

- **Active Sub-Network:** Which paths are active for input $x_s \in \mathbb{R}^{d_{in}}$? Choose a threshold τ_A close to 1. The paths that pass through gates in $\mathcal{G}_t^A(x_s, \tau_A)$ do not matter much in gate adaptation because they are already *on*, and are responsible for holding the memory for input $x_s \in \mathbb{R}^{d_{in}}$. In particular, (4) evaluates close to 0 for such paths because $\left| \frac{\partial G_{x_s, \Theta_t^g}(l, p(l))}{\partial \theta^g(m)} \right| < \frac{d\chi_\varepsilon(v)}{dv} \Big|_{v=\chi_\varepsilon^{-1}(v)}$.

- **Active Sub-Network:** Which paths are learning for input $x_s \in \mathbb{R}^{d_{in}}$? Those paths that have one gate from $\mathcal{G}_t^S(x_s, \tau_S)$ and the rest of $(d-2)$ gates from the set $\mathcal{G}_t^A(x_s, \tau_A)$. For such paths, the magnitude of at least one of the $(d-1)$ terms in (4) will be greater than $\tau_S(\tau_A)^{(d-2)}$, and the rest of the $(d-2)$ terms will contain a $\frac{d\chi_\varepsilon(v)}{dv} \Big|_{v=\chi_\varepsilon^{-1}(v)}$ component and hence will contribute less to the summation.

- **Role of β** for now is limited to an analytical convenience, especially to address the non-differentiability artefact in ReLU gates. The ideas is that as $\beta \rightarrow \infty$, the analysis applies more sharply to networks with ReLU gates. ‘

4. Related Work

(Du et al., 2018) show that in fully connected DNNs with $w = \Omega(\text{poly}(n)2^{O(d)})$, and in residual neural networks (ResNets) with $w = \Omega(\text{poly}(n, d))$ gradient descent converges to zero training loss. (Du et al., 2018) claim to demystify the second part of what we called the depth phenomena (“why deeper networks are harder to train”), since, the dependence on the number of layers improves exponentially for ResNets. Our optimisation results analytically are weaker than (Du et al., 2018) in the sense that we consider only DGNs with decoupling assumptions. However, we show both parts of the depth phenomena, in particular why increasing depth till a point helps training.

In comparison (Fiat et al., 2019) who were the first to initiate the study on GaLU networks, we believe, our work has made significant progress. We introduced adaptable gates and show via experiments that gate adaptation is key in learning, thereby showing a clear separation between GaLU and ReLU networks. To support the claim, we have used idea from (Arora et al., 2019), in that, we measure $\nu_t = y^\top K_t^{-1} y$ to show that the Eigen spaces indeed align with respect to the labelling function.

In comparison to (Frankle and Carbin, 2018), we also show in our experiments that the winning lottery is in the gating pattern, which in the case of ReLU networks is inseparable from the weights. However, our experiments show that the weights can be reinitialised if we have the learned gating pattern.

5. Conclusion

In this paper, we introduced two important conceptual novelties namely deep gated networks (DGNs) and “path-view”, to obtain additional insights about gradient descent in deep learning. Using these two novel concepts, we achieved the following:

- (i) resolution to the depth phenomena for DGNs under decoupling assumption. In particular, our results showed that increasing depth is equivalent to whitening of data and increasing depth beyond a point degrades the spectrum of the Gram matrix at initialisation.
- (ii) each input example has a corresponding active sub-network, which are learned when the gates adapt.
- (iii) a preliminary theory to analyse gate adaptation. Our analysis points out to the presence of two complementary networks for each input example, one being the active sub-network which holds the memory for that input example and the other being the sensitivity sub-network of gates that are adapting.
- (iv) we looked at various DGNs with adaptable gates and we observed in experiments that the adaptable/learned gates generalise better than non-adapting/non-learned gates.

Based on our theory and experiments, we conclude that :

- (a) *Hidden features are in the active sub-networks*, which are in turn decided by the gates.
- (b) *Understanding generalisation would involve a study of gate adaptation.*

References

Sanjeev Arora, Simon S. Du, Wei Hu, Zhiyuan Li, and Ruosong Wang. Fine-grained analysis of optimization and generalization for overparameterized two-layer neural networks. *CoRR*, abs/1901.08584, 2019. URL <http://arxiv.org/abs/1901.08584>.

Simon S Du and Wei Hu. Width provably matters in optimization for deep linear neural networks. *arXiv preprint arXiv:1901.08572*, 2019.

Simon S Du, Jason D Lee, Haochuan Li, Liwei Wang, and Xiyu Zhai. Gradient descent finds global minima of deep neural networks. *arXiv preprint arXiv:1811.03804*, 2018.

Jonathan Fiat, Eran Malach, and Shai Shalev-Shwartz. Decoupling gating from linearity. *CoRR*, abs/1906.05032, 2019. URL <http://arxiv.org/abs/1906.05032>.

Jonathan Frankle and Michael Carbin. The lottery ticket hypothesis: Finding sparse, trainable neural networks. *arXiv preprint arXiv:1803.03635*, 2018.

Chiyuan Zhang, Samy Bengio, Moritz Hardt, Benjamin Recht, and Oriol Vinyals. Understanding deep learning requires rethinking generalization. *arXiv preprint arXiv:1611.03530*, 2016.

6. Paths

Vectorised Notation: Given a dataset $(x_s, y_s)_{s=1}^n \in \mathbb{R}^{d_{in} \times \mathbb{R}}$, let data be represented as matrices $x \in \mathbb{R}^{d_{in} \times \cdot}$ and $y \in \mathbb{R}^n$ with the convention that $x_s = x(\cdot, s) \in \mathbb{R}^{d_{in}}$ and $y_s = y(s) \in \mathbb{R}$. For the purpose of this section we follow the vectorised notation in Table 5.

Input layer	$x(s, i, 0) = x(i, s)$
Pre-activation	$q_t(s, i, l) = \Theta(l, \cdot, i)^\top x_t(s, \cdot, l - 1)$
Layer output	$x_t(s, i, l) = q_t(s, i, l)G_t(s, i, l)$
Final output	$\hat{y}_t(x) = \Theta_t(d, \cdot, 1)^\top x_t(s, \cdot, d - 1)$

Table 5. A deep gated network in the vectorised form. $l = 1, \dots, d - 1$ denote the intermediate layers.

The idea behind the “path view” is to regard the given neural network as multitude of connections from input to output. We now describe the zeroth and first order terms in the language of paths.

Definition 6.1 (Neural Path). *Let $\mathcal{P} = [d_{in}] \times [w]^{d-1}$ be a cross product of index sets. Define a path p by $p \stackrel{\text{def}}{=} (p(0), p(1), \dots, p(d - 1)) \in \mathcal{P}$, where $p(0) \in [d_{in}]$, and $p(l) \in [w], \forall l \in [d - 1]$.*

A path p starts at an input node $p(0)$ goes through nodes $p(l)$ in layer $l \in [d - 1]$ and finishes at the output node.

Definition 6.2. [Strength] Each path is also associated with a strength given by: $w_t(p) = \prod_{l=1}^d \Theta_t(l, p(l - 1), p(l))$

Definition 6.3. [Activation Level] The activity of a path p for input s is given by: $A(s, p) = \prod_{l=1}^d G(s, p(l), l)$

In the case when $G \in \{0, 1\}$ it also implies that $A \in \{0, 1\}$.

Definition 6.4. [Neural Feature] Given a gating pattern \mathcal{G}_t , define

$$\phi_{x_s, \mathcal{G}_t}(p) \stackrel{\text{def}}{=} x(p(0), s)A_{\mathcal{G}_t}(x_s, p), \quad (5)$$

and let $\phi_{x_s, \mathcal{G}_t} = (\phi_{x_s, \mathcal{G}_t}(p), p \in [P]) \in \mathbb{R}^P$ be the hidden feature corresponding to input x_s . Let $\Phi_{x, \mathcal{G}_t} = [\phi_{x_1, \mathcal{G}_t} | \dots | \phi_{x_n, \mathcal{G}_t}] \in \mathbb{R}^{P \times n}$ be the feature matrix obtained by stacking the features $\phi_{x_s, \mathcal{G}_t}$ of inputs $x_s \in \mathbb{R}^{d_{in}}$ column-wise.

6.1. Results in Section 2

Lemma 6.1.

$$K_t(s, s') = \sum_{i=1}^{d_{in}} x(i, s)x(i, s')\kappa_t(s, s', i), \text{ where}$$

$$\kappa_t(s, s', i) \stackrel{\text{def}}{=} \sum_{\substack{p_1, p_2 \in P: \\ p_1, p_2 \rightsquigarrow i}} A(x_s, p_1)A(x_{s'}, p_2)\langle \varphi_{t, p_1}, \varphi_{t, p_2} \rangle$$

Proof. Note that

$$\hat{y}_t(x_s) = \sum_{p \in \mathcal{P}} x(p(0), s)A(x_s, p)w_t(p)$$

Differentiating with respect to any of the weights $\theta(m), m \in [d_{net}]$, we have

$$\begin{aligned} \frac{\partial \hat{y}_t(x_s)}{\partial \theta(m)} &= \frac{\partial \sum_{p \in \mathcal{P}} x(p(0), s)A(x_s, p)w_t(p)}{\partial \theta(m)} \\ \Psi_t(m, s) &= \sum_{p \in \mathcal{P}} x(p(0), s)A(x_s, p) \frac{\partial w_t(p)}{\partial \theta(m)} \\ &= \sum_{p \in \mathcal{P}} x(p(0), s)A(x_s, p)\varphi_{t, p}(m) \end{aligned}$$

Since, only the path strengths are changing, the Gram matrix K_t is given by

$$\begin{aligned}
K_t(s, s') &= \Psi_t(\cdot, s)^\top \Psi_t(\cdot, s') \\
&= \sum_{m=1}^{d_{net}} \Psi_t(m, s) \Psi_t(m, s') \\
&= \sum_{m=1}^{d_{net}} \left(\sum_{p_1 \in \mathcal{P}} x(p_1(0), s) A(x_s, p_1) \varphi_{t, p_1}(m) \right) \left(\sum_{p_2 \in \mathcal{P}} x(p_2(0), s') A(x_{s'}, p_2) \varphi_{t, p_2}(m) \right) \\
&= \sum_{m=1}^{d_{net}} \sum_{\substack{p_1, p_2 \in \mathcal{P}: \\ p_1, p_2 \rightsquigarrow \theta(m)}} x(p_1(0), s) A(x_s, p_1) x(p_2(0), s') A(x_{s'}, p_2) \varphi_{t, p_1}(m) \varphi_{t, p_2}(m) \\
&= \sum_{i=1}^{d_{in}} \sum_{\substack{p_1, p_2 \in \mathcal{P}: \\ p_1, p_2 \rightsquigarrow i}} x(p_1(0), s) A(x_s, p_1) x(p_2(0), s') A(x_{s'}, p_2) \langle \varphi_{t, p_1}, \varphi_{t, p_2} \rangle \\
&= \sum_{i=1}^{d_{in}} \sum_{\substack{p_1, p_2 \in \mathcal{P}: \\ p_1, p_2 \rightsquigarrow i}} x(i, s) A(x_s, p_1) x(i, s') A(x_{s'}, p_2) \langle \varphi_{t, p_1}, \varphi_{t, p_2} \rangle \\
&= \sum_{i=1}^{d_{in}} x(i, s) x(i, s') \sum_{\substack{p_1, p_2 \in \mathcal{P}: \\ p_1, p_2 \rightsquigarrow i}} A(x_s, p_1) A(x_{s'}, p_2) \langle \varphi_{t, p_1}, \varphi_{t, p_2} \rangle
\end{aligned}$$

□

Lemma 6.2. Under Assumption 1, 2 we have for paths $p, p_1, p_2 \in \mathcal{P}, p_1 \neq p_2$, at initialisation we have (i) $\mathbb{E}[\langle \varphi_{0, p_1}, \varphi_{0, p_2} \rangle] = 0$, (ii) $\langle \varphi_{0, p}, \varphi_{0, p} \rangle = d\sigma^{2(d-1)}$

Proof.

$$\langle \varphi_{t, p_1}, \varphi_{t, p_2} \rangle = \sum_{m=1}^{d_{net}} \varphi_{t, p_1}(m) \varphi_{t, p_2}(m)$$

Let $\theta(m), m \in [d_{net}]$ be any weight such that $p \rightsquigarrow \theta(m)$, and w.l.o.g let $\theta(m)$ belong to layer $l' \in [d]$. If either $p_1 \not\rightsquigarrow \theta(m)$ or $p_2 \not\rightsquigarrow \theta(m)$, then it follows that $\varphi_{t, p_1}(m) \varphi_{t, p_2}(m) = 0$. In the case when $p_1, p_2 \rightsquigarrow \theta(m)$, we have

$$\begin{aligned}
&\mathbb{E}[\varphi_{0, p_1}(m) \varphi_{0, p_2}(m)] \\
&= \mathbb{E} \left[\prod_{\substack{l=1 \\ l \neq l'}}^d \left(\Theta_0(l, p_1(l-1), p_1(l)) \Theta_0(l, p_2(l-1), p_2(l)) \right) \right] \\
&= \prod_{\substack{l=1 \\ l \neq l'}}^d \mathbb{E}[\Theta_0(l, p_1(l-1), p_1(l)) \Theta_0(l, p_2(l-1), p_2(l))]
\end{aligned}$$

where the $\mathbb{E}[\cdot]$ moved inside the product because at initialisation the weights (of different layers) are independent of each other. Since $p_1 \neq p_2$, in one of the layers $\tilde{l} \in [d-1], \tilde{l} \neq l'$ they do not pass through the same weight, i.e.,

$\Theta(\tilde{l}, p_1(\tilde{l}-1), p_1(\tilde{l}))$ and $\Theta(\tilde{l}, p_2(\tilde{l}-1), p_2(\tilde{l}))$ are distinct weights. Using this fact

$$\begin{aligned}
& \mathbb{E} [\varphi_{0,p_1}(m) \varphi_{0,p_2}(m)] \\
&= \prod_{\substack{l=1 \\ l \neq l', \tilde{l}}}^d \mathbb{E} [\Theta_0(l, p_1(l-1), p_1(l)) \Theta_0(l, p_2(l-1), p_2(l))] \\
&= \mathbb{E} [\Theta_0(\tilde{l}, p_1(\tilde{l}-1), p_1(\tilde{l}))] \mathbb{E} [\Theta_0(\tilde{l}, p_2(\tilde{l}-1), p_2(\tilde{l}))] \\
&= 0
\end{aligned}$$

The proof of (ii) is complete by noting that $\sum_{m=1}^{d_{net}} \varphi_{t,p}(m) \varphi_{t,p}(m)$ has d non-zero terms for a single path p and at initialisation we have

$$\begin{aligned}
& \varphi_{0,p}(m) \varphi_{0,p}(m) \\
&= \prod_{\substack{l=1 \\ l \neq l'}}^d \Theta_0^2(l, p(l-1), p(l)) \\
&= \sigma^{2(d-1)}
\end{aligned}$$

□

Theorem 6.3. *Let*

$$\mu(s, s', i) \stackrel{def}{=} \sum_{p \in P: p \rightsquigarrow i} A(x_s, p) A(x_{s'}, p),$$

then under Assumptions 1, 2 it follows that

$$\begin{aligned}
\mathbb{E} [\lambda_0(s, s', i)] &= d\sigma^{2(d-1)} \mu(s, s', i) \\
\mathbb{E} [K_0(s, s')] &= d\sigma^{2(d-1)} \sum_{i=1}^{d_{in}} x(i, s) x(i, s') \mu(s, s', i) \\
\text{Var}[K_0] &\leq O \left(d_{in}^2 \sigma^{4(d-1)} \max\{d^2 w^{2(d-2)+1}, d^3 w^{2(d-2)}\} \right)
\end{aligned}$$

Proof.

$$\begin{aligned}
\mathbb{E} [\lambda_0(s, s', i)] &= d\sigma^{2(d-1)} \mu(s, s', i) \\
\mathbb{E} [K_0(s, s')] &= d\sigma^{2(d-1)} \sum_{i=1}^{d_{in}} x(i, s) x(i, s') \mu(s, s', i)
\end{aligned}$$

The above two claims follow from the algebraic expression for K_t and Lemma 2.1. We now look at the variance calculation. The idea is that we expand $\text{Var}[K_0(s, s')] = \mathbb{E}[K_0(s, s')^2] - \mathbb{E}[K_0(s, s')]^2$ and identify the terms which cancel due to subtraction and then bound the rest of the terms.

Let $\theta(m)$ belong to layer $l'(m)$, then

$$\begin{aligned}
\mathbb{E}[K_0(s, s')] &= \sum_{m=1}^{d_{net}} \mathbb{E} \left[\left(\sum_{p_1 \in P} x(p_1(0), s) A(s, p_1) \frac{\partial w_\Theta(p_1)}{\partial \theta(m)} \right) \left(\sum_{p_2 \in P} x(p_2(0), s) A(s', p_2) \frac{\partial w_\Theta(p_2)}{\partial \theta(m)} \right) \right] \\
&= \sum_{m=1}^{d_{net}} \mathbb{E} \left[\sum_{p_1, p_2 \in P} x(p_1(0), s) A(s, p_1) \frac{\partial w_\Theta(p_1)}{\partial \theta(m)} x(p_2(0), s') A(s', p_2) \frac{\partial w_\Theta(p_2)}{\partial \theta(m)} \right] \\
&= \sum_{m=1}^{d_{net}} \sum_{\substack{p_1, p_2 \in P \\ p_1, p_2 \sim \theta(m)}} x(p_1(0), s) A(s, p_1) x(p_2(0), s') A(s', p_2) \mathbb{E} \left[\prod_{\substack{l=1 \\ l \neq l'(m)}}^{d-1} \Theta(l, p_1(l-1), p_1(l)) \Theta(l, p_2(l-1), p_2(l)) \right] \\
&\stackrel{(a)}{=} \sum_{m=1}^{d_{net}} \sum_{\substack{p_1, p_2 \in P \\ p_1, p_2 \sim \theta(m)}} x(p_1(0), s) A(s, p_1) x(p_2(0), s') A(s', p_2) \prod_{\substack{l=1 \\ l \neq l'(m)}}^{d-1} \mathbb{E} [\Theta(l, p_1(l-1), p_1(l)) \Theta(l, p_2(l-1), p_2(l))] \\
\end{aligned} \tag{6}$$

where (a) follows from the fact that at initialisation the layer weights are independent of each other. Note that the right hand side of (6) only terms with $p_1 = p_2$ will survive the expectation.

In the expression in (7) note that $p_1 = p_2$ and $p_3 = p_4$.

$$\begin{aligned}
\mathbb{E}[K_0(s, s')]^2 &= \\
&\left(\sum_{m=1}^{d_{net}} \sum_{\substack{p_1, p_2 \in P \\ p_1, p_2 \sim \theta(m)}} x(p_1(0), s) A(s, p_1) x(p_2(0), s') A(s', p_2) \prod_{\substack{l=1 \\ l \neq l'(m)}}^{d-1} \mathbb{E} [\Theta(l, p_1(l-1), p_1(l)) \Theta(l, p_2(l-1), p_2(l))] \right) \\
&\left(\sum_{m'=1}^{d_{net}} \sum_{\substack{p_3, p_4 \in P \\ p_3, p_4 \sim \theta(m')}} x(p_3(0), s) A(s, p_3) x(p_4(0), s') A(s', p_4) \prod_{\substack{l=1 \\ l \neq l'(m')}}^{d-1} \mathbb{E} [\Theta(l, p_3(l-1), p_3(l)) \Theta(l, p_4(l-1), p_4(l))] \right) \\
&= \\
&\sum_{m, m'=1}^{d_{net}} \sum_{\substack{p_1, p_2, p_3, p_4 \in P \\ p_1, p_2 \sim \theta(m) \\ p_3, p_4 \sim \theta(m')}} \left[\left(x(p_1(0), s) A(s, p_1) x(p_2(0), s') A(s', p_2) x(p_3(0), s) A(s, p_3) x(p_4(0), s') A(s', p_4) \right) \right. \\
&\quad \left(\prod_{\substack{l=1 \\ l \neq l'(m')}}^{d-1} \mathbb{E} [\Theta(l, p_1(l-1), p_1(l)) \Theta(l, p_2(l-1), p_2(l))] \mathbb{E} [\Theta(l, p_3(l-1), p_3(l)) \Theta(l, p_4(l-1), p_4(l))] \right) \\
&\quad \left(\mathbb{E} [\Theta(l, p_1(l'(m')-1), p_1(l'(m')))] \Theta(l, p_2(l'(m')-1), p_2(l'(m'))) \right) \\
&\quad \left. \left(\mathbb{E} [\Theta(l, p_3(l'(m)-1), p_3(l'(m)))] \Theta(l, p_4(l'(m)-1), p_4(l'(m))) \right) \right] \\
\end{aligned} \tag{7}$$

In the expression in (8), paths p_1, p_2, p_3, p_4 do not have constraints, and can be distinct.

$$\begin{aligned}
\mathbb{E} [K_0^2(s, s')] = & \sum_{m, m'=1}^{d_{net}} \sum_{\substack{p_1, p_2 \sim \theta(m) \\ p_3, p_4 \sim \theta(m')}} \left[\left(x(p_1(0), s) A(s, p_1) x(p_2(0), s') A(s', p_2) x(p_3(0), s) A(s, p_3) x(p_4(0), s') A(s', p_4) \right) \right. \\
& \left(\prod_{\substack{l=1 \\ l \neq l'(m')}}^{d-1} \mathbb{E} [\Theta(l, p_1(l-1), p_1(l)) \Theta(l, p_2(l-1), p_2(l)) \Theta(l, p_3(l-1), p_3(l)) \Theta(l, p_4(l-1), p_4(l))] \right) \\
& \left(\mathbb{E} [\Theta(l, p_1(l'(m')-1), p_1(l'(m')) \Theta(l, p_2(l'(m')-1), p_2(l'(m')))] \right) \\
& \left. \left(\mathbb{E} [\Theta(l, p_3(l'(m)-1), p_3(l'(m))) \Theta(l, p_4(l'(m)-1), p_4(l'(m)))] \right) \right] \\
& (8)
\end{aligned}$$

We now state the following facts/observations.

- **Fact 1:** Any term that survives the expectation (i.e., does not become 0) and participates in (8) is of the form $\sigma^{4(d-1)}(x(p_1(0), s) A(s, p_1) x(p_2(0), s') A(s', p_2) x(p_3(0), s) A(s, p_3) x(p_4(0), s') A(s', p_4))$, where p_1, p_2, p_3, p_4 are free variables, and participates in (7) is of the form $\sigma^{4(d-1)}(x(p_1(0), s) A(s, p_1) x(p_2(0), s') A(s', p_2) x(p_3(0), s) A(s, p_3) x(p_4(0), s') A(s', p_4))$, where $p_1 = p_2, p_3 = p_4$.
- **Fact 2:** The number of paths through a particular weight $\theta(m)$ in one of the middle layers is $d_{in} w^{d-3}$, and the number of paths through a particular weight $\theta(m)$ in either the first or the last layer is $d_{in} w^{d-2}$.
- **Fact 3:** Let \mathcal{P}' be an arbitrary set of paths constrained to pass through some set of weights. Let \mathcal{P}'' be the set of paths obtained by adding an additional constraint that the paths also should pass through a particular weight say $\theta(m)$. Now, if $\theta(m)$ belongs to :

1. a middle layer, then $|\mathcal{P}''| = \frac{|\mathcal{P}'|}{w^2}$.
2. the first layer or the last layer, then $|\mathcal{P}''| = \frac{|\mathcal{P}'|}{w}$.

- **Fact 4:** For any p_1, p_2, p_3, p_4 combination that survives the expectation in (8) can be written as

$$\begin{aligned}
& \left(\prod_{\substack{l=1 \\ l \neq l'(m')}}^{d-1} \mathbb{E} [\Theta(l, p_1(l-1), p_1(l)) \Theta(l, p_2(l-1), p_2(l)) \Theta(l, p_3(l-1), p_3(l)) \Theta(l, p_4(l-1), p_4(l))] \right) \\
& \left(\mathbb{E} [\Theta(l, p_1(l'(m')-1), p_1(l'(m')) \Theta(l, p_2(l'(m')-1), p_2(l'(m')))] \right) \\
& \left(\mathbb{E} [\Theta(l, p_3(l'(m)-1), p_3(l'(m))) \Theta(l, p_4(l'(m)-1), p_4(l'(m)))] \right) \\
& = \\
& \left(\prod_{\substack{l=1 \\ l \neq l'(m')}}^{d-1} \Theta_0^2(l, \rho_a(l-1), \rho_a(l)) \Theta_0^2(l, \rho_b(l-1), \rho_b(l)) \right) \\
& \left(\Theta_0^2(l, \rho_a(l'(m')-1), \rho_a(l'(m'))) \right) \\
& \left(\Theta_0^2(l, \rho_b(l'(m)-1), \rho_b(l'(m))) \right),
\end{aligned}$$

where $\rho_a \rightsquigarrow \theta(m)$ and $\rho_b \rightsquigarrow \theta(m')$ are what we call as *base* (case) paths.

- **Fact 5:** For any given base paths ρ_a and ρ_b there could be multiple assignments possible for p_1, p_2, p_3, p_4 .
- **Fact 6:** Terms in (8), wherein, the base case is generated as $p_1 = p_2 = \rho_a$ and $p_3 = p_4 = \rho_b$ (or $p_1 = p_2 = \rho_b$ and $p_3 = p_4 = \rho_a$), get cancelled with the corresponding terms in (7).
- **Fact 7:** When the bases paths ρ_a and ρ_b do not intersect (i.e., do not pass through the same weight in any one of the layers), the only possible assignment is $p_1 = p_2 = \rho_a$ and $p_3 = p_4 = \rho_b$ (or $p_1 = p_2 = \rho_b$ and $p_3 = p_4 = \rho_a$), and such terms are common in (8) and (7), and hence do not show up in the variance term.
- **Fact 7:** Let base paths ρ_a and ρ_b cross at layer $l_1, \dots, l_k, k \in [d-1]$, and let $\rho_a = (\rho_a(1), \dots, \rho_a(k+1))$ where $\rho_a(1)$ is a sub-path string from layer 1 to l_1 , and $\rho_a(2)$ is the sub-path string from layer l_1+1 to l_2 and so on, and $\rho_a(k+1)$ is the sub-path string from layer l_k+1 to the output node. Then the set of paths that can occur in $\mathbb{E}[K_0(s, s')^2]$ are of the form:

1. $p_1 = p_2 = \rho_a, p_3 = p_4 = \rho_b$ (or $p_1 = p_2 = \rho_b, p_3 = p_4 = \rho_a$) which get cancelled in the $\mathbb{E}[K_0(s, s')^2]$ term.
2. $p_1 = \rho_a, p_3 = \rho_b, p_2 = (\rho_b(1), \rho_a(2), \rho_a(3), \dots, \rho_a(k+1)), p_4 = (\rho_a(1), \rho_b(2), \rho_b(3), \dots, \rho_b(k+1))$, which are obtained by splicing the base paths in various combinations. Note that for such spliced paths $p_1 \neq p_2$ and $p_3 \neq p_4$ and hence do not occur in the expression for $\mathbb{E}[K_0(s, s')^2]$ in (7).

- **Fact 8:** For k crossings of the base paths there are 4^{k+1} splicings possible, and those many terms are extra in the $\mathbb{E}[K_0(s, s')^2]$ calculation in (8) comparison to the $\mathbb{E}[K_0(s, s')^2]$ calculation. We now enumerate cases of possible crossings, and reason out the magnitude of their contribution to the variance term using the **Fact 1** to **Fact 8**.

Case 1 $k = 1$ crossing in either first or last layer. There are $2w$ weights in the first and the last layer, and the number of base path combinations is $w^{d-2} \times w^{d-2}$, and for each of these cases, m, m' could take $O(d^2)$ possible values. And the multiplication of the weights themselves contribute to $\sigma^{4(d-1)}$. Putting them together we have

$$d_{in}^2 \sigma^{4(d-1)} \times (2w) \times d^2 \times (w^{d-2} \times w^{d-2}) \times 4^2 = 32d_{in}^2 \sigma^{4(d-1)} d^2 w^{2(d-2)+1}$$

Case 2 $k = 1$ crossing in one of the middle layers. There are $w^2(d-2)$ weights in the first and the last layer, and the number of base path combinations is $w^{d-3} \times w^{d-3}$, and for each of these cases, m, m' could take $O(d^2)$ possible values. And the multiplication of the weights themselves contribute to $\sigma^{4(d-1)}$. Putting them together we have

$$d_{in}^2 \sigma^{4(d-1)} \times w^2(d-2) \times d^2 \times (w^{d-3} \times w^{d-3}) \times 4^2 \leq 16d_{in}^2 \sigma^{4(d-1)} d^3 w^{2(d-3)}$$

Case 3 $k = 2$ crossings one in the first layer and other in the last layer. This case can be covered using Case 1 and then further restricting that the base paths should also in the other layer. So, we have

$$32d_{in}^2 \sigma^{4(d-1)} d^2 w^{2(d-2)+1} \times \underbrace{w}_{\text{possible weights in other layer}} \times \underbrace{w^{-1} \times w^{-1}}_{\text{reduction in paths due to additional restriction}} \times 4 = (32d_{in}^2 \sigma^{4(d-1)} d^2 w^{2(d-2)+1}) \times (4w^{-1}),$$

where the 4 is for the 4 extra possible ways of splicing the base paths.

Case 4 $k = 2$ crossings first one in the first layer or the last layer, and the second one in the middle layer. This can be obtained by looking at the Case 1 and then adding the further restriction that the base paths should cross each other in the middle layer.

$$32d_{in}^2 \sigma^{4(d-1)} d^2 w^{2(d-2)+1} \times w^2(d-2) \times (w^{-2}w^{-2}) \times 4 = (32d_{in}^2 \sigma^{4(d-1)} d^2 w^{2(d-2)+1}) \times (4dw^{-2})$$

Case 5 $k = 2$ crossings in the middle layer. This can be obtained by taking Case 2 and then adding the further restriction that the base paths should cross each other in the middle layer.

$$16d_{in}^2 \sigma^{4(d-1)} d^3 w^{2(d-3)} \times w^2(d-2) w^{-2} w^{-2} \times 4 \leq (16d_{in}^2 \sigma^{4(d-1)} d^3 w^{2(d-3)}) \times (4dw^{-2})$$

Case 6 $k = 3$ crossings first one in the first layer or the last layer, and the other two in the middle layers. This can be obtained by considering Case 4 and then adding the further restriction that the base paths should cross each other in the middle layer.

$$(32d_{in}^2 \sigma^{4(d-1)} d^2 w^{2(d-2)+1}) \times (4dw^{-2}) \times (4dw^{-2})$$

Case 7 $k = 3$ crossings first two in the first and last layers and the third one in the middle layers. This can be obtained by considering Case 3 and then adding the further restriction that the base paths should cross each other in the middle layer.

$$(32d_{in}^2 \sigma^{4(d-1)} d^2 w^{2(d-2)+1}) \times (4w^{-1}) \times (4dw^{-2})$$

Case 8 $k = 3$ crossings in the middle layer. This can be obtained by considering Case 5 and then adding the further restriction that the base paths should cross each other in the middle layer.

$$(16d_{in}^2 \sigma^{4(d-1)} d^3 w^{2(d-3)}) \times (4dw^{-2}) \times (4dw^{-2})$$

The cases can be extended in a similar way, increasing the number of crossings. Now, assuming $\frac{4d}{w^2} < 1$, the bounds in the various terms can be lumped together as below:

- We can add the bounds for Case 1, Case 4, Case 6 and other cases obtained by adding more crossings (one at a time) in the middle layer to Case 6. This gives rise to a term which is upper bounded by

$$d_{in}^2 \sigma^{4(d-1)} d^2 w^{2(d-2)+1} \left(\frac{1}{1 - 4dw^{-2}} \right)$$

- We can add the bounds for Case 3, Case 7 and other cases obtained by adding more crossings (one at a time) in the middle layer to Case 6. This gives rise to a term which is upper bounded by

$$d_{in}^2 \sigma^{4(d-1)} d^3 w^{2(d-2)} \left(\frac{1}{1 - 4dw^{-2}} \right)$$

- We can add the bounds for Case 2, Case 5, Case 8 and other cases obtained by adding more crossings (one at a time) in the middle layer to Case 6. This gives rise to a term which is upper bounded by

$$d_{in}^2 \sigma^{4(d-1)} d^2 w^{2(d-2)} \left(\frac{1}{1 - 4dw^{-2}} \right)$$

Putting together we have the variance to be bounded by

$$Cd_{in}^2 \sigma^{4(d-1)} \max\{d^2 w^{2(d-2)+1}, d^3 w^{2(d-2)}\},$$

for some constant $C > 0$. □

Lemma 6.4. *Under Assumption 1, 2 and gates sampled iid $Ber(p)$, we have, $\forall s, s' \in [n]$*

- (i) $\mathbb{E}_p [\lambda_0(s, s)] = \bar{\lambda}_{self} = d(pw)^{d-1}$
- (ii) $\mathbb{E}_p [\lambda_0(s, s')] = \bar{\lambda}_{cross} = d(p^2 w)^{d-1}$

Proof. The proof of (i) follows by noting that the average number of gates that are *on* in each layer is (pw) , and there are $(pw)^{d-1}$ paths starting from a given input node $i \in [d_{in}]$ and ending at the output node. The proof of (ii) follows by noting that on an average $p^2 w$ gates overlap per layer for two different inputs. □

Lemma 6.5. *Under Assumptions 1, 2, in soft-GaLU networks we have: (i) $\mathbb{E}[K_0] = \mathbb{E}[K_0^w] + \mathbb{E}[K_0^a]$, (ii) $\mathbb{E}[K_0^w] = \sigma^{2(d-1)}(x^\top x) \odot \lambda$, (iii) $\mathbb{E}[K_0^a] = \sigma^{2d}(x^\top x) \odot \delta$*

Proof. Follows from Lemma 2.1, and noting that Θ_0^g and Θ_0^w are iid. □

7. Deep Linear Networks

In this case, $G(s, l, i) = 1, \forall s \in [n], i \in [w], l \in [d-1]$. Note that all the paths are always active irrespective of which input is presented to the DLN. We can define the effective weight that multiplies each of the input dimensions as $\eta_t(i) \stackrel{\text{def}}{=} \sum_{p \in P: p(0)=i} w_t(p), i \in [d_{in}]$. Using the above definition of $\eta = (\eta(i), i \in [d_{in}]) \in \mathbb{R}^{d_{in}}$, the hidden feature representation can be simplified as $\hat{y}_t = \Phi_{x, 1}^\top w_t = x^\top \eta_t$. Thus it is clear that the DLN does not provide any high dimensional feature representation and the input features are retained as such. All that the depth adds is just a non-linear re-parameterisation of the weights. Also note that since $A(s, p) = 1, \forall p$ it follows that $\lambda_t^{s, s'}(i) = \lambda_t(i), \forall s, s' \in [n]$. Thus the Gram matrix can be reduced to $K_t = x^\top \Lambda_t x$, where Λ_t is an $d_{in} \times d_{in}$ diagonal matrix whose diagonal entries are $\lambda_t(i)$.

Corollary 7.1. *Under Assumption 2, for a DLN with $d_{in} = 1$, and dataset with $n = 1$ we have,*

$$\mathbf{E}_\Theta [K_0] = d(w\sigma^2)^{(d-1)} \quad (9)$$

Experiment 1: We consider a dataset with $n = 1$ and $(x, y) = (1, 1)$. We consider $\mathcal{N}(1_\dagger, \Theta_t)$, for $d_{in} = 1, w = 100$, and $d = 2, 4, 6, 8, 10$. We set $\sigma = \sqrt{\frac{1}{w}}$ and the weights are drawn according to Assumption 2. We set the learning rate to be $\alpha = \frac{0.1}{d}$, and for this setting we expect the error dynamics to be the following $\frac{e_{t+1}^2}{e_t^2} = 0.81$. The results are shown in Figure 15. We observe that irrespective of the depth the error dynamics is similar (since $\alpha = \frac{0.1}{d}$). However, we observe faster (in comparison to the ideal rate of 0.81) convergence of error to zero since the magnitude of K_t increases with time (see Figure 15).

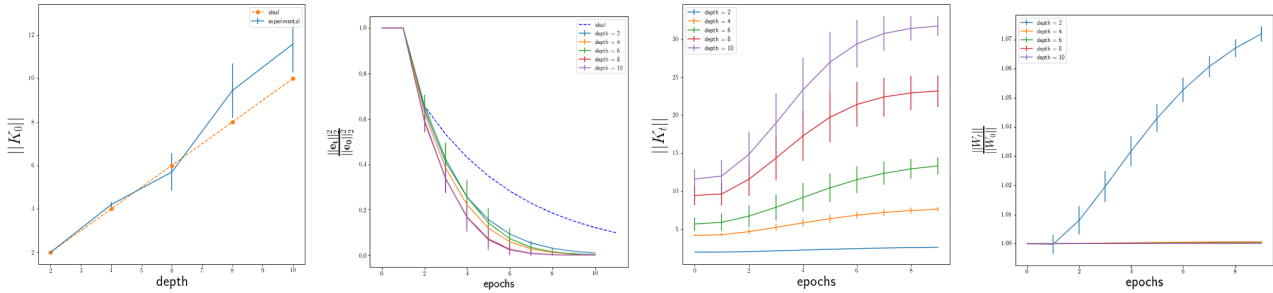


Figure 15. In all the plots $d_{in} = 1, n = 1, w = 100, \sigma^2 = \frac{1}{w}$ averaged over 5 runs. The left most plot shows K_0 as a function of depth. The second from left plot shows the convergence rate. The third plot from left shows the growth of K_t over the course of training, and the right most plot shows the growth of weights (L_2 -norm) with respect to time.